HHS Public Access

Author manuscript

ChemMedChem. Author manuscript; available in PMC 2016 October 12.

Published in final edited form as:

ChemMedChem. 2016 September 20; 11(18): 1978–1982. doi:10.1002/cmdc.201600301.

Near-Infrared Intraoperative Chemiluminescence Imaging

Dr. Gabriel E. Büchel[a],[b], **Brandon Carney**[a],[d], **Travis M. Shaffer**[c],[d], **Dr. Jun Tang**[a], **Dr. Christine Austin**[e], **Prof. Manish Arora**[e], **Prof. Brian M. Zeglis**[a],[d], **Prof. Jan Grimm**[a],[c],[f],[g], **Prof. Jörg Eppinger**[b], and **Prof. Thomas Reiner**[a],[f]

Jörg Eppinger: jorg.eppinger@kaust.edu.sa; Thomas Reiner: reinert@mskcc.org

[a]Department of Radiology, Memorial Sloan Kettering Cancer Center, New York, NY 10065 (USA)

[b]King Abdullah University of Science and Technology (KAUST), KAUST-Catalysis Center (KCC), Thuwal 23955-6900 (Saudi Arabia)

[c]Molecular Pharmacology Program, Memorial Sloan Kettering Cancer Center, 1275 York Avenue, New York, NY 10065 (USA)

[d]Department of Chemistry, Hunter College and PhD Program in Chemistry, The Graduate Center of the City University of New York, New York, NY 10018 (USA)

[e]Department of Preventive Medicine, Icahn School of Medicine at Mount Sinai, New York, NY 10029 (USA)

[f]Department of Radiology, Weill Cornell Medical College, New York, NY 10065 (USA)

[g]Program of Pharmacology, Weill Cornell Medical College, New York, NY 10065 (USA)

Abstract

Intraoperative imaging technologies recently entered the operating room, and their implementation is revolutionizing how physicians plan, monitor, and perform surgical interventions. In this work, we present a novel surgical imaging reporter system: intraoperative chemiluminescence imaging (ICI). To this end, we have leveraged the ability of a chemiluminescent metal complex to generate near-infrared light upon exposure to an aqueous solution of Ce^{4+} in the presence of reducing tissue or blood components. An optical camera spatially resolves the resulting photon flux. We describe the construction and application of a prototype imaging setup, which achieves a detection limit as low as 6.9 pmol cm^{-2} of the transition-metal-based ICI agent. As a proof of concept, we use ICI for the in vivo detection of our transition metal tracer following both systemic and subdermal injections. The very high signal-to-noise ratios make ICI an interesting candidate for the development of new intraoperative imaging technologies.

Glow in the dark

Correspondence to: Jörg Eppinger, `jorg.eppinger@kaust.edu.sa`; Thomas Reiner, `reinert@mskcc.org`.

Supporting information and the ORCID identification number(s) for the author(s) of this article can be found under http://dx.doi.org/10.1002/cmdc.201600301.

A preclinical imaging setup was developed to detect chemiluminescence in fresh tissues after intravenous or subdermal administration of a ruthenium metal complex. High signal-to-noise ratios were obtained without the need for excitation light. This could be a novel technology for intraoperative imaging and surgical margin evaluation.

Keywords

chemiluminescence; intraoperative imaging; lymph node imaging; near infrared; ruthenium

In vivo imaging has revolutionized diagnoses, monitoring, and treatment of disease. However, these technologies are often restricted to whole-body anatomic imaging, for example, providing physicians with the location of bulk tumor tissue on a macroscopic level.[1] Although this has improved the accuracy of surgical interventions and decreased impact on healthy tissues, most established imaging methods do not help operating surgeons answer a critical question that often arises during surgery: are there residual traces or other nests of tumor tissue remaining? While surgeons generally seek to leave narrow margins to have as little impact as possible on healthy tissue, this approach risks leaving residual tumor tissue behind, which can ultimately lead to recurrence of the disease, whereas over-aggressive surgery can lead to loss of function. Finding the right delicate balance in this struggle it is therefore a pressing clinical need. An answer to this problem could be intraoperative imaging technologies that can help physicians see residual tumor tissue within the surgical bed.[2]

Different technologies have been suggested and tested for their potential to serve as intraoperative margin-identifying tools, including optical fluorescence imaging,[3] detection of radioactive isotopes with β- or γ-detecting probes,[4] Raman spectroscopy,[5] and Cherenkov luminescence.[6] Ultimately, however, to date none of these have become a reliable standard-of-care tool that is used as routinely as whole-body PET, MRI, and CT imaging.

The generation of an imaging signal through chemiluminescence is fundamentally different from fluorescence imaging, as these chemiluminescent agents emit light *without* requiring an excitation light source. Typically, chemiluminescence imaging is based on the detection of photons produced as a by-product of the reduction/oxidation of a probe molecule. In biological systems, chemiluminescence imaging has only briefly been touched upon.[7] The most notable example is the injection of luminol into mice, which generates violet photons (424 nm) upon its oxidation by endogenous myeloperoxidase.[8]

However, transition-metal-mediated chemiluminescence has so far remained largely untapped by the molecular imaging community. Advantages of chemiluminescence over other methods include: 1) no excitation light necessary; 2) no tissue penetration issues for

incident light; 3) unlike in Cherenkov, no radioactivity is needed, eliminating exposure to patients and hospital personnel; 4) there are a large number of potential in vivo chemiluminescence imaging agents available, ranging from small organic molecules and transition-metal complexes to nanoparticles,[10] spanning wavelengths from the visible to the near-infrared (NIR) spectrum; and 5) these imaging agents can easily be conjugated to biologically active targeting molecules to target specific tissues, for example, which is one of the fundamental requirements for a molecular imaging agent.[11] In this proof-of-principle study, we show that high signal-to-noise ratios can be achieved by detecting the NIR photon that is emitted from the oxidation/reduction cycle of the reporter, that intraoperative chemiluminescence imaging reaches detection limits suitable for in vivo use, and that the biodistribution of a transition-metal-based chemiluminescent reporter can be visualized in vivo.

Figure 1 illustrates the generation and detection of a chemiluminescence signal under conditions suitable for intraoperative chemiluminescence imaging (ICI). Because application of the required oxidation agent to sample tissue is essential to elicit chemiluminescence, we developed the nebulizing device outlined in Figure 1A. It is designed to fit into a commercially available IVIS Spectrum imaging system (Figure 1B) and can be operated remotely via a cable when the IVIS Spectrum door is closed and camera shutters are open. The spray bottle contains an aqueous solution of the oxidizing agent $(NH_3)_2Ce(NO_3)_6$ and is aimed toward the tissue sample, a histological slide, or any other analyte (Figure 1C). Once a spray burst is released, the surface of the tissue of interest is covered in $(NH_3)_2Ce(NO_3)_6$, which will oxidize the ICI reporter contained in the tissue, prompting the emission of photons. Alternatively, if the $(NH_3)_2Ce(NO_3)_6$ solution is sprayed on a region lacking any ICI reporters, no photons will be generated. ICI is therefore devoid of autofluorescence and allows the mapping of the distribution of the ICI reporter close to the tissue surface. A detailed list of the used materials, instructions for assembly and photographs of the device (Figure S1) are compiled in the Supporting Information.

The highly water-soluble complex $[Ru(bpy)_3]^{2+}$ is a prime example of a potential transition-metal ICI reporter (Figure 2A), with reports on its chemiluminescence properties stretching back to 1966.[12] The emission band in the NIR range (ν~600 nm, Figure 2B) may be fine-tuned through modifications of the ligand environment.[13] It results from the relaxation of an excited $[Ru(bpy)_3]^{2+*}$ triplet state (τ=650 ns in water), which is accessible through photochemical excitation of $[Ru(bpy)_3]^{2+}$ or chemical reduction of $[Ru(bpy)_3]^{3+}$. In the presence of suitable oxidation and reducing agents, $[Ru(bpy)_3]^{2+}$ acts as single electron transfer (SET) redox catalyst, which partially emits the reaction energy in the form of photons (Figure 2C). We found that in the presence of tissue or serum, which act as reducing agent, low concentrations of Ce^{4+} are sufficient to initiate this $[Ru(bpy)_3]^{2+}$-catalyzed redox cycle resulting in a NIR signal.

While ICI does not require incident light, each $[Ru(bpy)_3]^{2+}$ complex can only emit one photon, which results in lower photon flux rates than produced by fluorophores. Therefore, the sensitivity of the experimental setup is of particular importance. In our case, we tested the minimum detectable amount of $[Ru(bpy)_3]^{2+}$ by mixing 100 μL of the metal complex solution (347 μmol to 6.9 pmol in water) and 100 μL of a solution of $(NH_3)_2Ce(NO_3)_6$ in

water (25 mM) on a microscope slide, and then spraying a solution of triethylamine (1:3 in water/ethanol (1:1), 0.24±0.04 mL per spray burst) onto the droplet. Figure 3A shows the resulting chemiluminescence at various concentration levels, with the quantified data plotted in Figure 3B. The minimum detectable signal (>3-fold over background) using our current apparatus was determined to be 6.9 pmol cm^{-2}.

We tested the general feasibility of ICI imaging in fresh tissues by injecting a solution of $[Ru(bpy)_3]Cl_2$ (8–33 nmol in 100 μL PBS) intravenously in a set of healthy mice (n=5); 10 min after injection, the mice were sacrificed, their body cavities were opened, kidneys cut, and chemiluminescence was generated by spraying $(NH_3)_2Ce(NO_3)_6$ onto the body cavities.

Not surprisingly, large amounts of signal were localized to kidneys (Figure 4A) and liver, whereas other organs did not emit significant chemiluminescence, indicating renal clearance of $[Ru(bpy)_3]^{2+}$. Kidney chemiluminescence is far greater within the tissue than the tissue surface, and organs did not emit chemiluminescence if not treated with the ICI agent (Figure 4B). Biodistribution of the reporter was established from a second cohort of mice (n=10), which underwent similar treatment. All major organs were excised, and the chemiluminescence in each organ was quantified individually. Comparison with signals generated when the animals were injected with PBS alone yields signal-to-noise ratios of 27/1 for kidney and 21/1 for liver (Figure 4C), and only moderate signal intensities were observed for other organs. This confirms the observed renal localization of the $[Ru(bpy)_3]^{2+}$ reporter. ICP-MS analyses of the mouse tissues further corroborated the ICI-based imaging data (Figure 4D). We found that ruthenium concentrations correlate well with photon flux rates, with the highest deposition in the kidneys (574 000 photons s^{-1} cm^{-2} sr^{-1} and 1.24±0.25 μg g^{-1}), followed by liver tissue (260 000 photons s^{-1} cm^{-2} sr^{-1} and 256±47 ng g^{-1}). Overall, this indicates that ICI might not only be useful to detect the presence of $[Ru(bpy)_3]^{2+}$ in vivo, but that this technique might ultimately be able to quantify concentrations noninvasively.

One major difficulty for many types of surgical interventions is the detection and removal of sentinel lymph nodes. Typically, sentinel lymph node detection is performed by injecting a detectable agent close to a tumor site, where it is transported by the lymphatic system into the sentinel lymph nodes.[14] While the agent therefore does not have to be targeted, strong imaging signals enhance precision and ease imaging signal identification. ICI could complement existing technologies and improve the identification and delineation of these tissues. To test the potential of ICI for lymph node detection, we injected $[Ru(bpy)_3]Cl_2$ (80 nmol in 10 μL in PBS) subdermally into the left hind paw of mice (n=5), whereas the right paw was injected with PBS alone. After 15 min, the mice were sacrificed, and the left and right popliteal lymph nodes on both sides were visualized with ICI (Figure 5A). The radiance observed for lymph nodes containing $[Ru(bpy)_3]^{2+}$ was 10±4.3-fold higher than for control lymph nodes (167 000 and 17 000 photons s^{-1} cm^{-2} sr^{-1} for positive and control lymph nodes, respectively, p<0.028, n=5, Figure 5B, C). While these values are similar to other approaches, this first proof-of-principle dataset indicates that this technology could indeed harbor clinically useful applications, maybe even in parallel with fluorescence imaging probes (Figure S2). Due to the typically lower signal intensity of chemiluminescence relative to traditional fluorophores, image generation in the operating

room would likely require the rigorous exclusion of NIR light, similar to what has already been established for Cherenkov imaging.[6] This, together with the development of tailor-made clinical instrumentation that allows both the administration of oxidizing agent together with high sensitivity photon detection, will be fundamental to successful clinical translation.

In summary, we show that ICI allows the detection of NIR photons down to thresholds of 6.9 pmol cm^{-2} and that ruthenium-based ICI agents can be used in vivo after systemic injection and subdermal application. Improving nebulizing and optical equipment, introduction of different metal complexes, and optimized exposure times would likely further decrease detection limits. We developed a preclinical imaging setup for applying ammonium cerium nitrate inside an IVIS Spectrum imaging system, which simulates the "spray-on" procedure a physician would likely perform in the operating room. Our ICI agent—$[Ru(bpy)_3]Cl_2$—is a well-known ruthenium-based transition-metal complex, which is highly water soluble and stable toward degradation in the bloodstream (Figure S3). $[Ru(bpy)_3]^{2+}$ can be modified with multiple types of linkers that can be used for bioconjugation,[15] including maleimides, amines, and NHS esters.[16]

The imaging protocol presented herein is a proof-of-principle study for ICI in living systems and could serve as a starting point for a variety of applications. The ruthenium complex may be linked to small molecules and peptides, to target and highlight specific markers and to help physicians delineate small lesions and surgical margins. Other approaches could involve encapsulating the highly water-soluble $[Ru(bpy)_3]^{2+}$ in nanomaterials and imaging a targeted lesion during its removal by the surgical team. We are confident that ICI is particularly appealing for surgical applications, and we believe that the described method can be adapted at low cost and with low technical barriers in many preclinical laboratories, potentially paving the way for clinical translation.

Supplementary Material

Refer to Web version on PubMed Central for supplementary material.

Acknowledgments

The authors thank Prof. Jason S. Lewis, Prof. Kayvan Keshari, and Dr. Neil Taunk for helpful discussions. We also thank Dr. Susanne Kossatz, Dr. Christian Brand, and Ms. Kimberley Fung for help with experiments, and Ms. Leah Bassity for editing the manuscript. Technical services provided by the MSKCC Small-Animal Imaging Core Facility, supported in part by the US National Institutes of Health (NIH) Cancer Center Support Grant P30 CA008748-48, are gratefully acknowledged. The authors thank the NIH (K25 EB016673 and R21 CA191679, T.R.; 4R00A178205-02, B.M.Z.; R01A183953 and R01EB014944 as well as R01CA183953, J.G.), the MSKCC Center for Molecular Imaging and Nanotechnology (T.R. and J.G.), the Tow Foundation (B.C.), the MSKCC Experimental Therapeutics Center (J.G.), the National Science Foundation Integrative Graduate Education and Research Traineeship (IGERT 0965983 at Hunter College for B.C. and T.M.S.) for their generous support. The research reported in this publication was supported by funding from the King Abdullah University of Science and Technology (KAUST). All animal experiments were done in accordance with protocols approved by the Institutional Animal Care and Use Committee of MSKCC and followed National Institutes of Health guidelines for animal welfare.

References

1. Fong, Y.; Giulianotti, PC.; Lewis, J.; Koerkamp, BG.; Reiner, T. Imaging and Visualization in the Modern Operating Room: A Comprehensive Guide for Physicians. Springer; New York: 2015.

2. a) Nguyen QT, Tsien RY. Nat Rev Cancer. 2013; 13:653. [PubMed: 23924645] b) Weissleder R, Pittet MJ. Nature. 2008; 452:580. [PubMed: 18385732]

3. van Dam GM, Themelis G, Crane LM, Harlaar NJ, Pleijhuis RG, Kelder W, Sarantopoulos A, de Jong JS, Arts HJ, van der Zee AG, Bart J, Low PS, Ntziachristos V. Nat Med. 2011; 17:1315. [PubMed: 21926976]

4. Heller S, Zanzonico P. Semin Nucl Med. 2011; 41:166. [PubMed: 21440694]

5. a) Zavaleta CL, Garai E, Liu JT, Sensarn S, Mandella MJ, Van de Sompel D, Friedland S, Van Dam J, Contag CH, Gambhir SS. Proc Natl Acad Sci USA. 2013; 110:E2288. [PubMed: 23703909] b) Harmsen S, Bedics MA, Wall MA, Huang R, Detty MR, Kircher MF. Nat Commun. 2015; 6:6570. [PubMed: 25800697]

6. a) Thorek DL, Abou DS, Beattie BJ, Bartlett RM, Huang R, Zanzonico PB, Grimm J. J Nucl Med. 2012; 53:1438. [PubMed: 22872741] b) Thorek DLJ, Riedl CC, Grimm J. J Nucl Med. 2014; 55:95. [PubMed: 24078721]

7. a) Lee JJ, White AG, Rice DR, Smith BD. Chem Commun. 2013; 49:3016.b) Lee D, Khaja S, Velasquez-Castano JC, Dasari M, Sun C, Petros J, Taylor WR, Murthy N. Nat Mater. 2007; 6:765. [PubMed: 17704780] c) Baumes JM, Gassensmith JJ, Giblin J, Lee JJ, White AG, Culligan WJ, Leevy WM, Kuno M, Smith BD. Nat Chem. 2010; 2:1025. [PubMed: 21107365]

8. Gross S, Gammon ST, Moss BL, Rauch D, Harding J, Heinecke JW, Ratner L, Piwnica-Worms D. Nat Med. 2009; 15:455. [PubMed: 19305414]

9. a) Hasan K, Bansal AK, Samuel IDW, Roldán-Carmona C, Bolink HJ, Zysman-Colman E. Sci Rep. 2015; 5:12325. [PubMed: 26179641] b) Sauvage JP, Collin JP, Chambron JC, Guillerez S, Coudret C, Balzani V, Barigelletti F, De Cola L, Flamigni L. Chem Rev. 1994; 94:993.c) Kodama K, Kobayashi A, Hirose T. Tetrahedron Lett. 2013; 54:5514.

10. a) McCapra F. Q Rev Chem Soc. 1966; 20:485.b) Vogler A, El-Sayed L, Jones RG, Namnath J, Adamson AW. Inorg Chim Acta. 1981; 53:L35.c) Akers, WJ. Nanomedicine: A Soft Matter Perspective. Pan, D., editor. CRC Press; Boca Raton, FL: 2014. p. 103-131.

11. Siraj N, El-Zahab B, Hamdan S, Karam TE, Haber LH, Li M, Fakayode SO, Das S, Valle B, Strongin RM. Anal Chem. 2016; 88:170. [PubMed: 26575092]

12. Hercules DM, Lytle FE. J Chem Soc. 1966; 88:4745.

13. Kerr E, Doeven EH, Barbante GJ, Hogan CF, Bower DJ, Donnelly PS, Connell TU, Francis PS. Chem Sci. 2015; 6:472.

14. a) Thorek DLJ, Ulmert D, Diop NFM, Lupu ME, Doran MG, Huang R, Abou DS, Larson SM, Grimm J. Nat Commun. 2014; 5:3097. [PubMed: 24445347] b) Chi C, Ye J, Ding H, He D, Huang W, Zhang GJ, Tian J. PLOS ONE. 2013; 8:e83927. [PubMed: 24358319] c) Ohnishi S, Lomnes SJ, Laurence RG, Gogbashian A, Mariani G, Frangioni JV. Mol Imaging. 2005; 4:172. [PubMed: 16194449] d) Bradbury MS, Phillips E, Montero PH, Cheal SM, Stambuk H, Durack JC, Sofocleous CT, Meester RJ, Wiesner U, Patel S. Integr Biol. 2013; 5:74.

15. a) James ML, Gambhir SS. Physiol Rev. 2012; 92:897. [PubMed: 22535898] b) Connell TU, James JL, White AR, Donnelly PS. Chem Eur J. 2015; 21:14146. [PubMed: 26264214]

16. a) Forster RJ, Bertoncello P, Keyes TE. Annual Rev Anal Chem. 2009; 2:359.b) Zhou X, Zhu D, Liao Y, Liu W, Liu H, Ma Z, Xing D. Nat Protoc. 2014; 9:1146. [PubMed: 24743421] c) Zanarini S, Rampazzo E, Bich D, Canteri R, Della Ciana L, Marcaccio M, Marzocchi E, Montalti M, Panciatichi C, Pederzolli C. J Phys Chem C. 2008; 112:2949.d) Liu R, Lv Y, Hou X, Yang L, Mester Z. Anal Chem. 2012; 84:2769. [PubMed: 22324291] e) Jantke D, Marziale AN, Reiner T, Kraus F, Herdtweck E, Raba A, Eppinger J. J Organomet Chem. 2013; 744:82.f) Reiner T, Jantke D, Marziale AN, Raba A, Eppinger J. Chemistry Open. 2013; 2:50. [PubMed: 24551533]

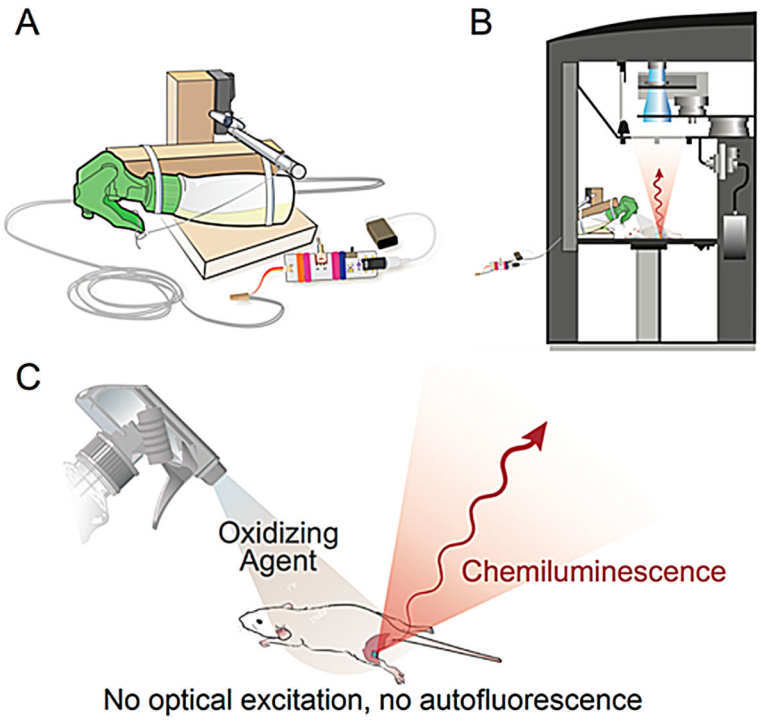

Figure 1.

Imaging setup and process for capturing intraoperative chemiluminescence. A) Schematic design of the automatic nebulizer designed for this application. B) Position of the spray device inside an IVIS Spectrum bioluminescence imaging system. C) Generation of near-infrared light by nebulizing and spraying on an oxidizing agent.

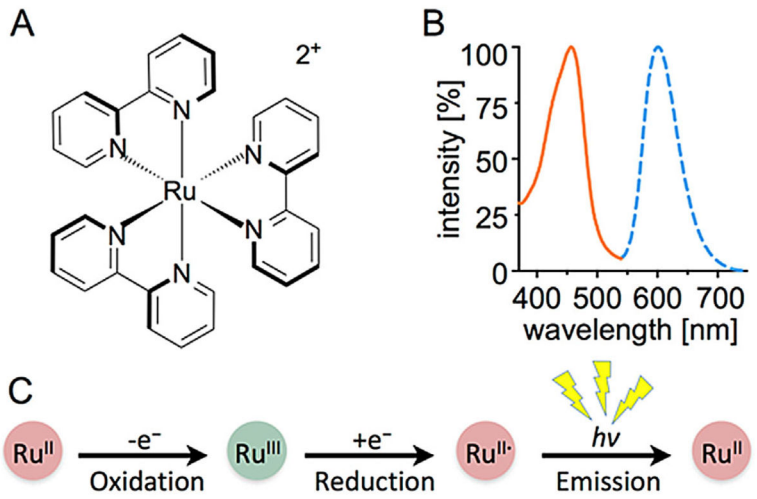

Figure 2.

$[Ru(bpy)_3]^{2+}$ structure, emission and reactivity. A) Structure and B) absorbance and emission spectrum of the ICI probe $[Ru(bpy)_3]^{2+}$. C) Reactivity of $[Ru(bpy)_3]^{2+}$. The probe, which is originally Ru^{II}, can be oxidized with $(NH_3)_2Ce(NO_3)_6$ to Ru^{III}, which is reduced to Ru^{II}*, an excited-state metal complex that emits a photon upon decay trough a normal fluorescence mechanism.

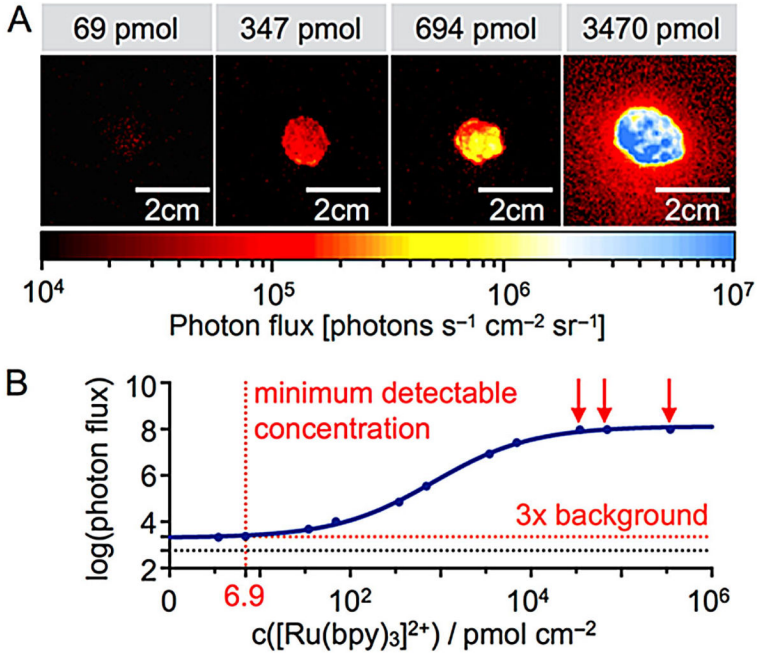

Figure 3.

Determining ICI sensitivity. A) Signal intensities at various concentrations of $[Ru(bpy)_3]^{2+}$ immobilized on a microscope slide after spraying on a mixture of $(NH_3)_2Ce(NO_3)_6$. B) Quantification of the imaging signals collected in panel A. The detection threshold (dashed line) was defined as 3× the background noise. Red arrows indicate concentrations at which the camera was saturated.

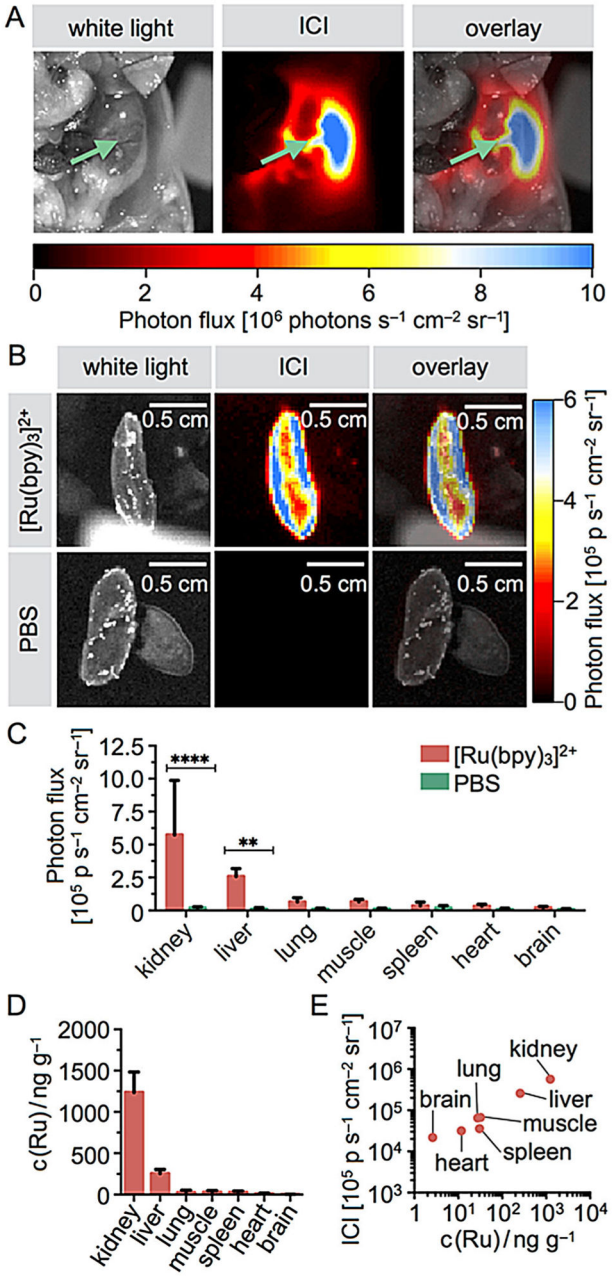

Figure 4.

In vivo abdominal surface chemiluminescence of $[Ru(bpy)_3]^{2+}$. The ICI agent was injected intravenously into healthy mice (26 nmol in 100 μL PBS), and the agent was allowed to clear from the bloodstream within 10 min. A) White light (left), ICI (center), and overlay (right) images of a mouse body cavity injected with 33 nmol of $[Ru(bpy)_3]^{2+}$ in 100 μL PBS. The green arrows point toward the right kidney. B) Images of excised kidneys are clearly visible in mice injected with the ICI agent, but not when injected with PBS. C) Quantification of the imaging results shown in panel A, with imaging quantification performed on excised organs. D) Quantification of ruthenium metal concentrations in

various tissues using ICP-MS. E) Correlation of ICI photon flux and ICP-MS determined ruthenium concentrations.

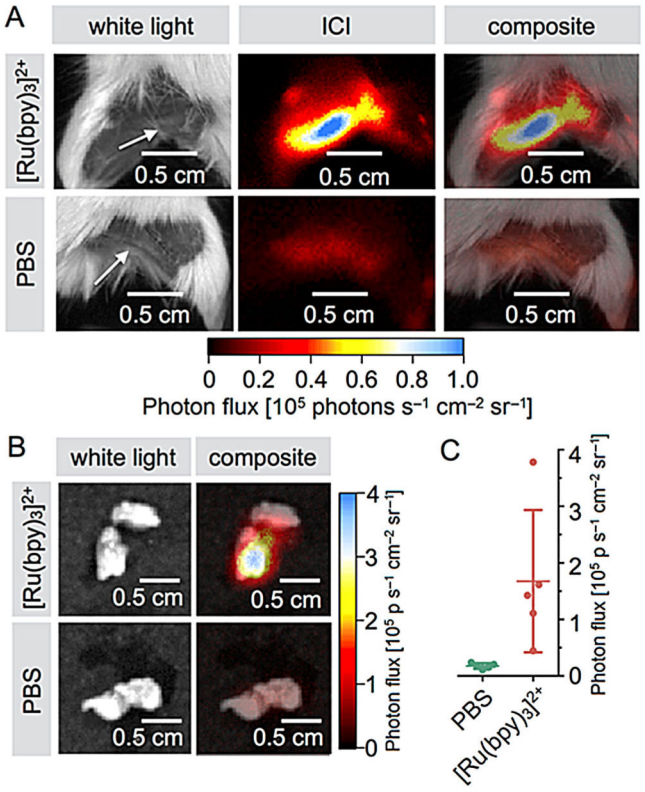

Figure 5.

Sentinel lymph node imaging with $[Ru(bpy)_3]^{2+}$. A) White light, chemiluminescence, and composite images of mice injected with $[Ru(bpy)_3]^{2+}$ (top) and PBS (bottom) into the hind limb (80 nmol in 10 μL PBS) and imaged 15 min after injection. B) Representative chemiluminescence signal in left popliteal lymph nodes (top row, white light and composite) and contralateral right lymph nodes (bottom row, white light and composite). C) Quantification of the chemiluminescence signal obtained for popliteal lymph nodes (n=5).